JOURNAL OF MATERIALS SCIENCE **35** (2000) 5553–5561

Improvement of microstructure and mechanical properties of AZ91/SiC composite by mechanical alloying

LÜ LI*, M. O. LAI, M. GUPTA, B. W. CHUA, A. OSMAN
Department of Mechanical and Production Engineering, The National University of Singapore, Singapore 119260
E-mail: mpeluli@nus.edu.sg

AZ91 magnesium alloy reinforced with SiC particulates was fabricated via powder metallurgy technique as well as mechanical alloying process where a planetary ball mill was employed. Microstructure and mechanical properties of the fabricated AZ91 composites had been evaluated. Microstructural study showed that grain size of the material was refined and SiC particulates were well distributed after mechanical alloying. Mechanical tests of the composite showed an enhanced yield and ultimate tensile strengths for the mechanically alloyed samples compared with those prepared via the powder metallurgical route.

1. Introduction

Magnesium is one of the lightest metallic materials available. Owing to its low density, Mg has been received much attention as an important structural material in recent years. The use of Mg is however limited due to its low stiffness, low strength, low wear resistance and high coefficient of thermal expansion. To enhance its mechanical properties and corrosion resistance, several alloying additions such as Al, Zn, Nd and Si have been used. Since the last decade, Mg based-metal matrix composites (MMCs) have been developed and manufactured using various techniques to achieve low density composites with high specific strength, stiffness and creep resistance even at elevated temperatures [1]. Additional advantages of Mg composites over unreinforced Mg alloys are improvement in the fatigue and wear resistance and a significant reduction in thermal expansion. Reinforcements used in Mg MMCs are in the form of either particles, short fibres or long fibres. Particle reinforced MMCs provide isotropic mechanical properties and low fabrication cost although the reinforcing effect is less than that using fibres as reinforcement. A volume fraction of at least 15–20% reinforcement is preferred for an effective increase of strength and stiffness in particle or short fibre reinforced Mg MMCs [2, 3]. For applications that require tensile creep strength, a short fibre reinforcement of advanced creep resistant Mg alloys is recommended. Squeeze casting may be considered as an economical method for producing short fibre reinforced Mg MMCs [2, 4].

There are in general two methods employed in the fabrication of Mg MMCs, namely, liquid process and solid process. In liquid process, the reinforcement particulates are mixed with molten Mg alloys by stirring while in solid process, the metallic powder and ceramic particulates are mechanically mixed followed by sintering. The major advantage of the liquid process is low cost and flexible in shape, but the solid process produces MMCs with good mechanical properties.

The major difficulty in the synthesis of Mg MMCs is the high reactivity of Mg. Some factors involved in from the fabrication process can cause degradation rather than improvement to the mechanical properties of the resulting composite. Special attentions must be given to the reaction products at the interface between SiC particles and the Mg matrix [5]. MgO may arise from oxide layer on the surface of the SiC as a result of heating during the fabrication, as well as from the reduction of oxides such as Al_2O_3. Although Al_2O_3 is stable in pure aluminium, it reacts with Mg in a Mg-Al alloy such that [6]:

$$3Mg + Al_2O_3 \leftrightarrow 3MgO + 2Al$$

$$3Mg + 4Al_2O_3 \leftrightarrow 3MgAl_2O_4 + 2Al$$

In addition to the oxide films, secondary phase particles, mainly Mg_2Si and $Al_{12}Mg_{17}$ have been observed. Mg_2Si in the form of fine particles that are occasionally of 10–400 nm in size, appears to originate from the reaction between the SiO_2 on the surface of SiC and the Mg matrix. Mg_2Si is believed to cause embrittlement. The reactions of the Mg_2Si are as follows [7, 8]:

$$2Mg + Si \rightarrow Mg_2Si$$

$$4Mg + SiO_2 \rightarrow Mg_2Si + 2MgO$$

* Author to whom all correspondence should be addressed.

Precipitation of the $Al_{12}Mg_{17}$ phase from solid solution in AZ91 Mg alloy takes place when the saturated alloy is aged. In general, the precipitate is in the form of fine platelets along the grains of the matrix alloy or as larger particles at the SiC/matrix interfaces.

Mechanical alloying (MA) or mechanical milling (MM) has been used [9] to improve the mechanical properties of Mg MMCs. The technique, although originally developed for the synthesis of oxide dispersion strengthening materials, has been widely used for synthesizing different kinds of metallic and non-metallic materials [10–12]. In this technique, powder particles are energetically milled in a vial. After MA or MM, very fine grain size with homogeneous structure can be obtained [13, 14]. The difficulty in MA is oxidation and contamination which may entirely affect the properties of the materials being milled [15]. Therefore a good control of the milling atmosphere and milling duration are critical.

The present investigation focuses on the influence of MA on microstructural evolution and the corresponding mechanical properties of Mg MMCs. Two different processing routes, namely, powder metallurgy (P/M) and MA, are used in the study.

2. Experimental procedures

Nominal composition of the base material used was Mg9%Al0.7%Zn0.15%Mn. Mg MMCs were fabricated via two different processing routes, conventional P/M and MA process. For the P/M process, 5 batches of MMC samples were fabricated via mixing the base metal with 10 vol.% of SiC of average particulate sizes of 15, 20, 25, 38 and 50 μm, respectively designated as PM1 to PM5. For the MA process, the base metal was first mixed with different amounts of SiC particulates, namely, 2, 4, 7 and 10 vol.%, designated as MA1 to MA4 respectively. 2 wt.% of stearic acid was used as a process control agent. MA was carried out in a planetary ball mill (Fritsh 5) at an angular rotational speed of 200 rpm. 40 g of powder mixture was used in each vial.

Hardened balls of 15 mm diameter with weight ratio of ball to powder mixture weight ratio of 20 : 1 were used. Before milling, the vials were filled with purified Ar to minimize oxidation of the milled powder. MA was carried out for different durations, after which the powder was collected in a glove box filled with Ar and directly loaded into a die for cold compaction. The cold compacts were later sintered at 450°C for 2 hours followed by extrusion at an extrusion ratio of 20 : 1. Structural changes of the extruded rods were monitored using a Shimadzu Lab-XRD-6000 x-ray diffraction (XRD) machine with Cu $K_{\alpha 1}$ radiation operated at 30 kV and 20 mA.

Tensile specimens were machined from the extruded rods to 6 mm diameter and 30 mm gauge length. Strain gauge of 25 mm was used to record the deformation of the specimens during tensile test. Tensile test was performed using an Instron 8500 at a strain rate of 0.027%/s.

3. Results and discussion

3.1. Microstructure

3.1.1. Powder metallurgically prepared MMC

Fig. 1 shows the microstructure of the matrix material in two orthogonal directions, namely, the transverse and longitudinal directions. The matrix consists of globular Mg grains with lamella $Al_{12}Mg_{17}$ decorating the grain boundaries (Fig. 1a). In the longitudinal direction, $Al_{12}Mg_{17}$ structure about few hundred microns long is aligned in the direction of extrusion (Fig. 1b). It is clear that the $Al_{12}Mg_{17}$ is coarse even after the extrusion. The average grain size of the matrix is 45 μm.

Figs 2 and 3 show the typical microstructure of PM1 and PM2 specimens respectively. The microstructure of the composite shows that some modifications to both the matrix grains and the eutectic $Al_{12}Mg_{17}$ phase have taken place. It is noted that $Al_{12}Mg_{17}$ precipitates are always located near the SiC particulates. This is the result of high stress field near SiC due to thermal mismatch between Mg matrix and the SiC particulate during the thermal process. It has been observed [16] that certain orientation relationship exists between $Al_{12}Mg_{17}$ and SiC, namely, $[111]_{Al_{12}Mg_{17}}//[\bar{1}101]_{SiC}$ and $(110)_{Al_{12}Mg_{17}}//(1120)_{SiC}$.

Instead of large globular grains, smaller grains with size of about 5 μm for the MMC reinforced with 15 μm SiC and 22 μm with 38 μm SiC have been presently

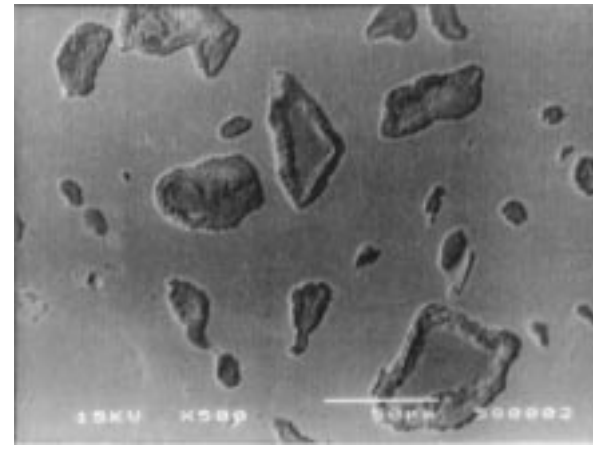

(a)

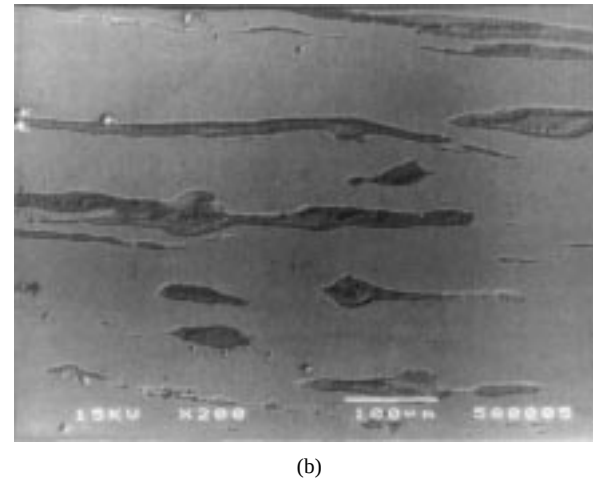

(b)

Figure 1 Microstrcture of base metal fabricated using P/M route.

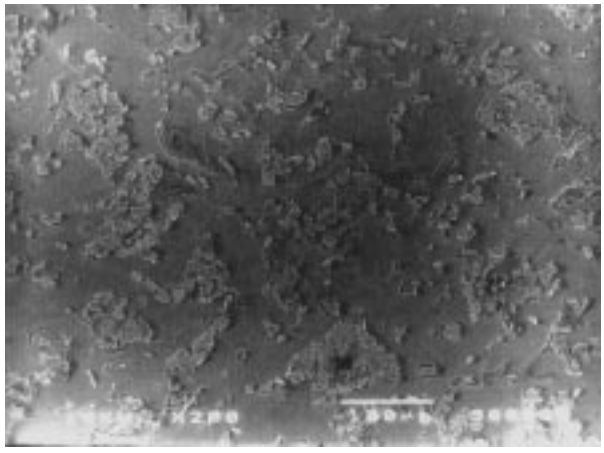

(a)

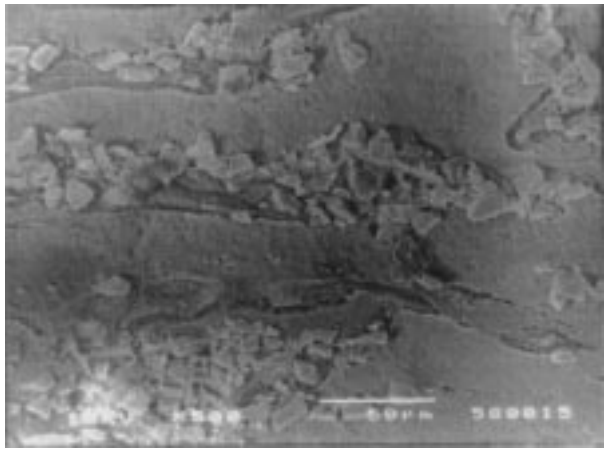

(b)

Figure 2 Microstructure of Mg alloy MMC reinforced with 15 μm SiC in (a) transverse direction and (b) longitudinal direction.

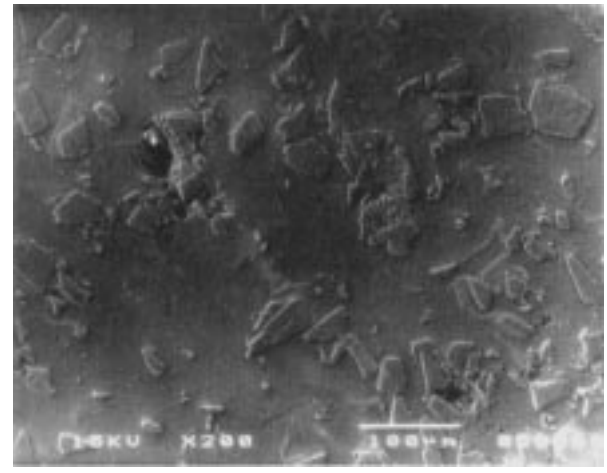

(a)

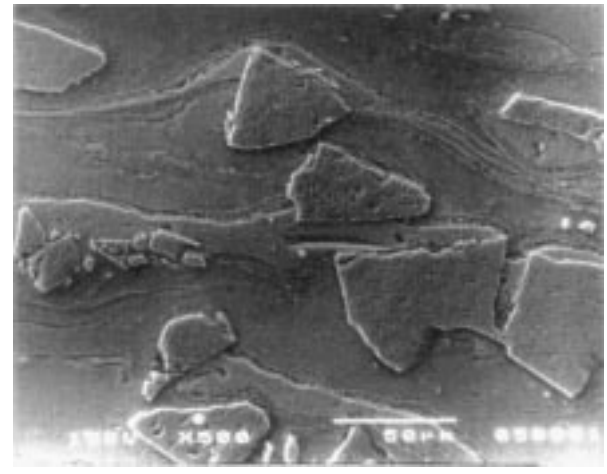

(b)

Figure 3 Microstructure of Mg alloy MMC reinforced with 50 μm SiC in (a) transverse direction and (b) longitudinal direction.

observed. It is clear that the presence of SiC has modified the structure of MMC. Average grain sizes of the MMC as a function of size of SiC particulates are shown in Fig. 4. It can be seen that the grain size decreases with the decrease in size of the SiC particulates. As grain boundaries possess a higher surface energy, grain generally tends to grow in order to minimize energy during sintering and solution treatment. When fine SiC particulates are used, the spacing between the particulates decreases resulting in strong pinning effect to resist grain growth. From the microstructures, the distribution of SiC particulates appears to be reasonably homogeneous although some clustering of particulates could be seen. Due to plastic flow of the matrix metal, SiC is aligned in the longitudinal direction together with the $Al_{12}Mg_{17}$ phase.

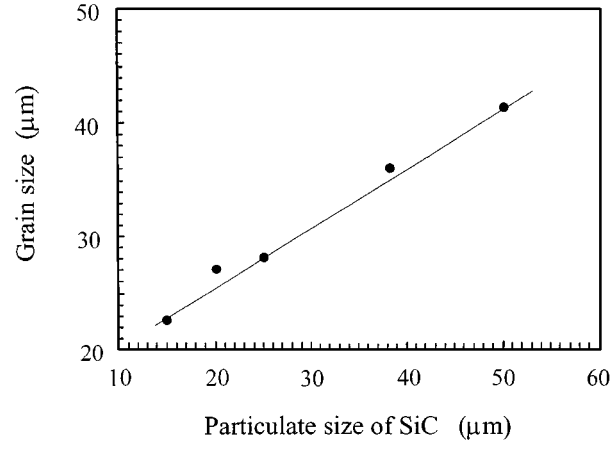

Figure 4 Grain size as a function of SiC particulate size.

3.1.2. Mechanically alloyed MMC

Fig. 5 shows the microstructure of MAed Mg matrix in the transverse direction where two phases of Mg and $Al_{12}Mg_{17}$ can be identified. Compared with the non-MAed MMC, much fine structure can be seen from the MAed counterpart. The fine structure is the result of the original large powder particles of Mg and Al being continuously fractured and cold welded during the MA process, thus causing a reduction in grain size. No large lamellar $Mg_{17}Al_{12}$ structure could be observed from the microstructure since Al has been mechanically dispersed into the Mg matrix. Although some big $Al_{12}Mg_{17}$ particles can still be observed from the microstructure, most of the particles are small. The existence of the big particles may probably be due to the short milling duration and Al has not been well distributed and refined.

Fig. 6a and b show the microstructures of the reinforced Mg MMC with different volume percentages of reinforcement in the transverse direction. Due to the repeated fracturing and rewelding process to break up

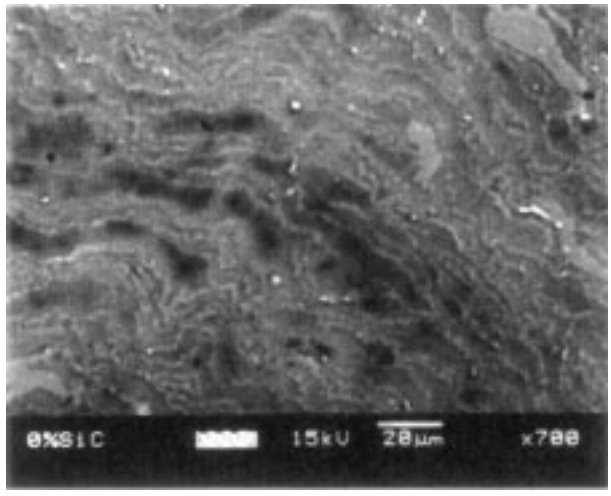

Figure 5 Microstructure of MAed AZ91 matrix.

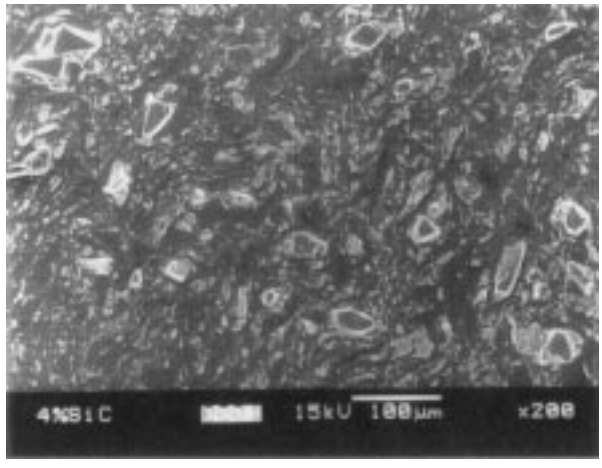

(a)

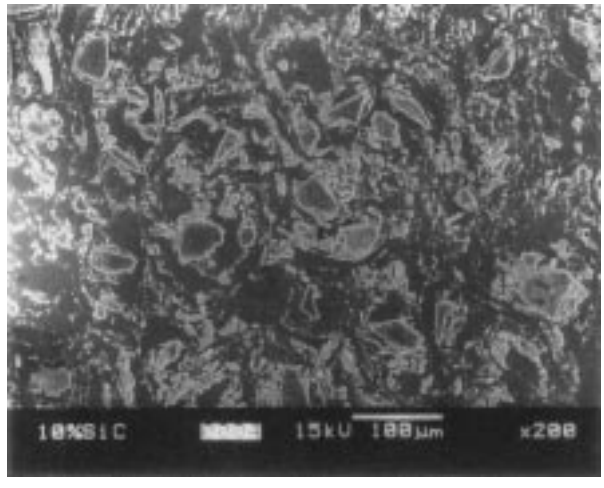

(b)

Figure 6 Microstructure of AZ91 base MMCs reinforced with different amounts of SiC: (a) 4 vol.% and (b) 10 vol.%.

the Mg and Al powders, a significant improvement in the distribution of SiC particulates in the matrix can be observed. At the same time, SiC particulates are also being fractured. Since these particulates are harder than Mg and Al powders, they get embedded into the matrix under collision. Only some clustering of SiC particulates in the composites could be detected as compared to that prepared by blending process.

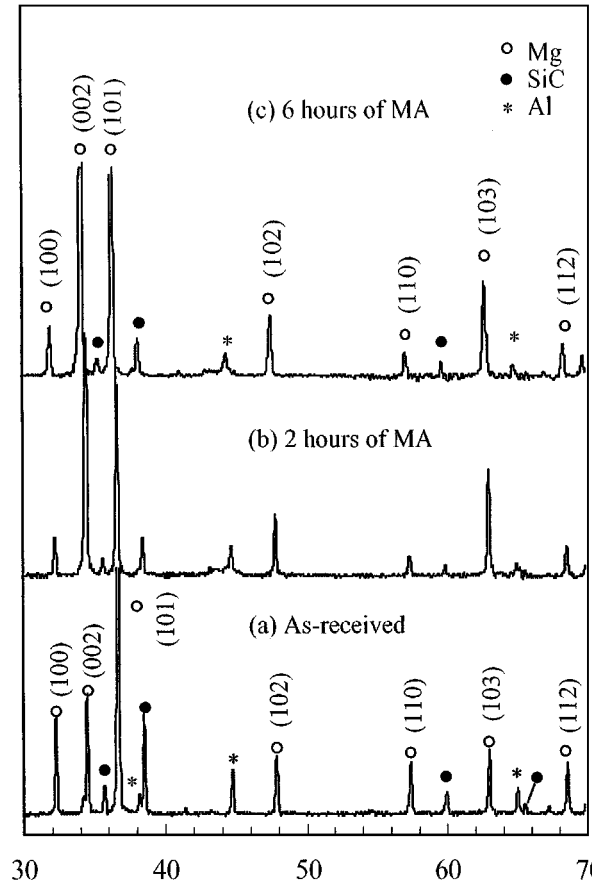

Figure 7 Structural evalution of MAed powders at different milling durations: (a) 0 hour, (b) 2 hours, (c) 6 hours.

Although the MAed MMC has been subjected to high temperature solution treatment, it still possesses fine magnesium grains with very fine intermetallic compounds forming along the grain boundaries, a result of the growth of grain size and $Mg_{17}Al_{12}$ being prohibited by the presence of dispersed fine oxide particles and SiC.

Results of structural investigation on the MAed powder mixture are shown in Fig. 7. As usual, Mg grain refinement is clearly indicated by the broadening of width of the Mg diffraction peak at its half maximum intensity. Although intensity of the Al diffraction peaks decreases, they can still be seen after 6 hours of MA indicating that Al has not fully been dissoluted into Mg. Longer milling duration may lead to further dissolution of Al into Mg but contamination of Fe from the milling tools may take place because of the existence of hard SiC particulates. It may therefore be better to shorten the duration of MA once homogenization has been reached. The diffraction peaks of SiC can also be observed to decrease as the duration of milling increases.

The decrease in intensity of SiC diffraction is attributed to the reduction of SiC particulate size. Structure of the MAed and extruded Mg specimen after solutionising is given in Fig. 8a. With disappearance of Al peaks, it is clear that Al has been fully dissoluted into the Mg. Formation of $Al_{12}Mg_{17}$ can be detected after ageing the solutionised Mg MMC, but as its amount of $Al_{12}Mg_{17}$ is relatively low and the strongest (330) peak overlaps with the Mg (101) peak, only low diffraction peaks can be seen in Fig. 8b.

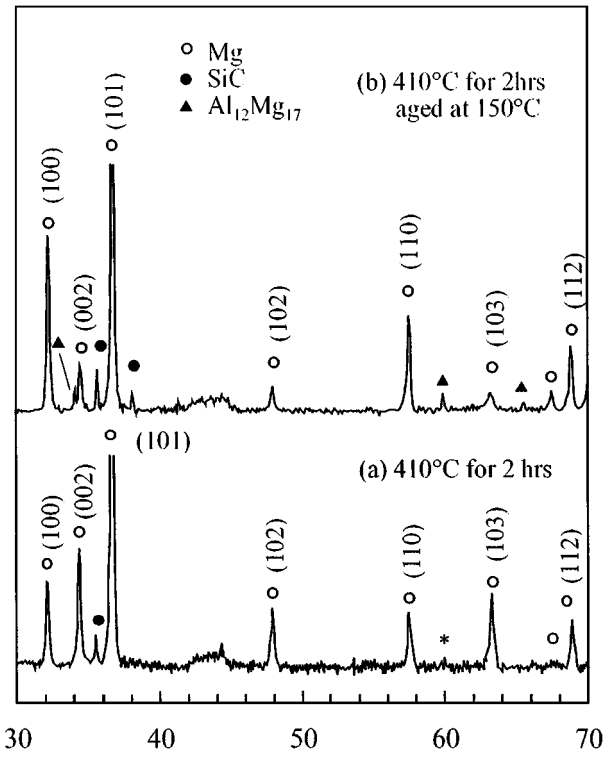

Figure 8 Structural changes in AZ91/4wt.%SiC specimen: (a) after solutionising at 410°C and (b) after solutionising at 410°C and ageing at 150°C.

3.2. Effect of aging

3.2.1. Powder metallurgically prepared MMC

Fig. 9 shows the variation of hardness of the non-MAed MMC as a function of ageing duration. The mean hardness value reveals that the MMCs achieve their peak ageing at about 15 hours. However, the increase in hardness after ageing is not significant as compared to the hardness of the solutionised specimens. The reason may be that after being given a precipitation hardening heat treatment, an incoherent coarse precipitate of $Al_{12}Mg_{17}$ was produced without the formation of GP zone or an intermediate metastable precipitate. Study has shown that the precipitate formed in an ageing hardened Mg-9%Al alloy consisted coarse $Al_{12}Mg_{17}$ plates lying on the basal planes of the matrix. Since the precipitate which appears in discontinuous form is not fine and dense enough, it is unable to produce a significant strengthening effect.

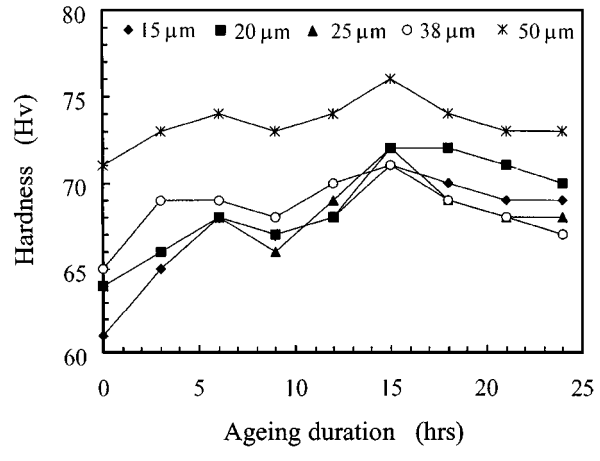

Figure 9 Variation of hardness with aging time at 168°C for unreinforced and reinforced composites of various sizes of SiC.

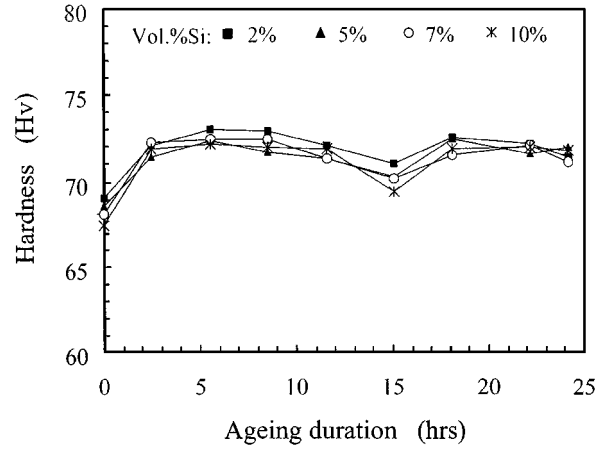

Figure 10 Variation of hardness with aging duration at 168°C.

The present results show that the MMCs reinforced with larger SiC particulates have relatively higher mean hardness value as compared to those with smaller SiC particulates. This hardness increase may be attributed to the probability of the hardness indentor hitting onto a larger particle was much higher than smaller particulates.

3.2.2. Mechanically alloyed MMC

Fig. 10 shows the hardness of the MAed specimens where it can be seen that the MMCs achieve peak age at about 6 hours, much shorter than that of conventionally processed specimens. This is because the structure of the MAed specimen is generally finer compared to the original non-MAed structure. By the repeated cold welding and fracturing of the matrix, the end product possesses a fine and uniform dispersion of reinforcement material even though the internal stress field could be higher than that in non-MAed specimens. It is generally found that ageing duration is shortened when the internal energy is high. However, the increase in hardness after aging was not significant as compared to the solutionised specimens. The same trend has also been observed in MAed Al alloys [17, 18]. This phenomenon is believed to be associated with the dominating effect of dispersion strengthening. The major difference between non-MAed and MAed specimens is the difference in grain size. In general, large effect of precipitation hardening can be obtained if precipitation takes place within the grains. The MA process causes more areas of grain boundary to be formed. Precipitation takes place more readily in the area of grain boundary leading to low hardening effect.

Compared with Fig. 9, the overall hardness of the MAed MMCs is higher than that of conventional non-MAed MMCs. This is most likely due to the effect of small grain size and well distributed SiC. It is also noted that as the volume of SiC particulates increased, almost no difference in hardness among MA1 to MA4 specimens could be detected, suggesting that the highest hardness have been achieved.

3.3. Mechanical properties

Fig. 11 shows the tensile test results in terms of 0.2% yield strength (YS), ultimate tensile strength (UTS) and Young's modulus for the non-MAed specimens. As can be seen from the figure, the 0.2% YS and UTS of the specimens decrease with the increase in SiC particulate size. Young's moduli of the specimens are found to remain almost constant with respect to the size of SiC.

Elongation measurement in Fig. 12 shows that the effect of size of SiC on the ductility of the MMC is minimal. In general, in the range measured, size of SiC does not strongly affect the ductility of the specimens. Based on theoretical consideration, fracture toughness is a function of Young's modulus, tensile strength and particle spacing. Although increase in particle spacing may lead to an increase in fracture ductility, the decrease in yield stress and Young's modulus may cause a decrease in ductility. Therefore the overall effect on ductility due to increasing particle spacing and decreasing yield stress and Young's modulus is neutralized.

The mechanical properties of MAed specimens are summarised in Fig. 13. Several features can be observed:

(i) Both 0.2%YS and UTS of the MAed specimens are almost 80% higher than those of non-MAed ones;

(ii) Both 0.2%YS and UTS decrease with the increase in volume of SiC particulates;

(iii) Young's moduli increase as the amount of SiC was increased. Overall, the Young moduli are higher as compared to the non-MAed specimens.

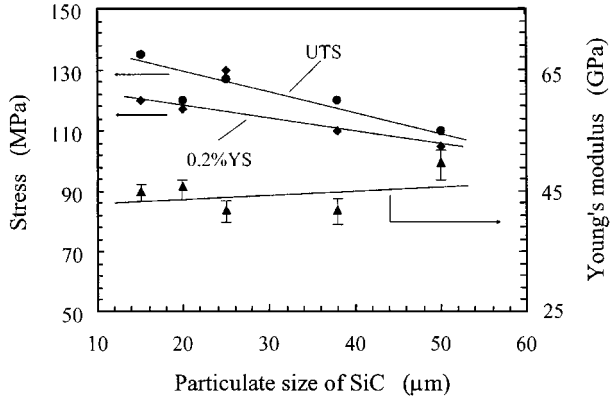

Figure 11 0.2%YS, UTS and modulus of non-MAed MMC.

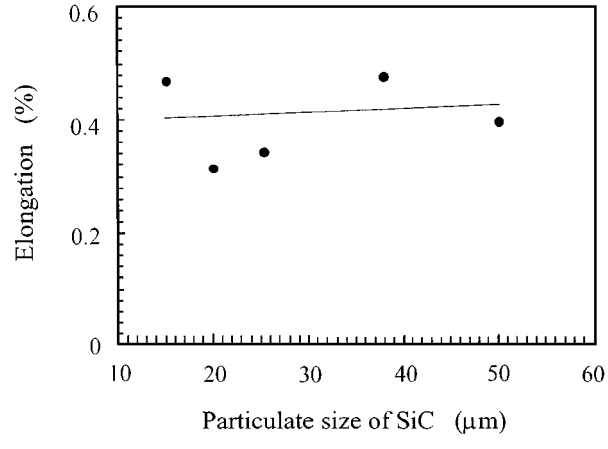

Figure 12 Elongation as a function of size of SiC.

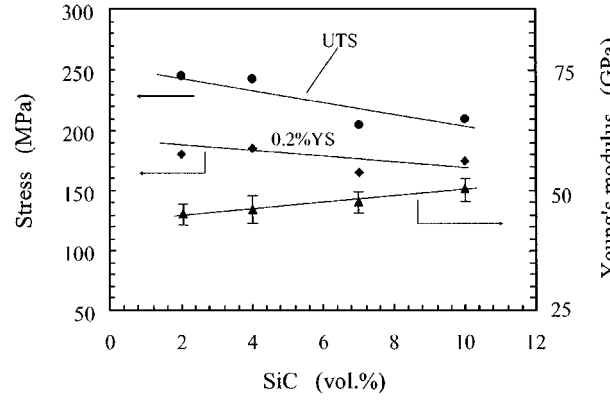

Figure 13 0.2%YS, UTS and modulus of MAed MMC.

Several factors can contribute to the enhanced mechanical properties. Firstly, in the MA process, grains are refined by repeated fracturing. Submicron and even nano-sized grains can be formed by the process. The small grains contain large grain boundary area which acts as obstacle to dislocation slip by limiting the slip distance. The boundaries prevent easy passage of slip from one grain to another resulting in dislocation pile-up. Mabuchi *et al.* [19] studied the mechanical properties of ingot metallurgical (I/M) and rapidly solidified (R/S) Mg-Si alloys and found that the yield strength of R/S material was about 4 to 5 times higher than that of I/M material. Based on Hall-Petch equation, it is known that yield stress, σ, is a function of grain size, d, as

$$\sigma = \sigma_0 + Kd^{-1/2} \tag{1}$$

where σ_0 is the stress to move dislocations and, K is a constant.

Developed from Taylor's theory, Armstrong *et al.* [20] showed that constant K is proportional to the square of Taylar factor M and to the shear stress τ_c as:

$$K \propto M^2 \tau_c \tag{2}$$

The value of M can be determined by finding the combination of slip systems that minimized the summation of shear strain but still satisfies the required continuity at the grain boundaries. Since less slip systems are available in a hcp structure of Mg alloy, the value of M for Mg is larger than that of fcc structure of Al [19, 20]. From Equations 1 and 2 it can be seen that the yield stress of Mg is strongly influenced by Taylar's factor M. When M is large, the influence of grain size on yield stress becomes a dominant factor. Therefore, for Mg alloys, grain size is important parameter to improve mechanical properties.

Secondly, the ball milling process also reduces SiC particulate size by high energy collision. It is known that strength of MMCs is associated with the spacing between reinforcement particulates. When the size of particulate is reduced causing a reduction in spacing between the particulates, an increase in resistance to the movement of dislocations will be caused. Lastly, ball milling may introduce extra reinforcement particulates

such as MgO due to oxidation which is almost unavoidable owing to the presence and increase in surface area of Mg particles with milling process. All these factors will contribute to the increase in strength of the MMC.

Strangely, it was found that 0.2%YS and UTS decreased as the SiC content increased (Fig. 13). One of the possible reasons could be the low extrusion ratio used which was unable to reduce defects such as voids. When high volume of SiC is used, defects become an important factor. In the ball milling process, since the size of the Mg particle is small, surface area per unit volume of particle is thus very large. Lo *et al*. [5] has found that as a result of the high reactivity of Mg, SiC has been observed to react with Mg. SiC particles are frequently separated from the matrix by an interfacial film composed of nanocrystalline MgO particles (10–70 nm diameter) to a depth depending upon conditions of fabrication. These films, which can be up to 500 nm in thickness, will promote interparticle fracture. The formation of MgO is due to the presence of oxide layer on the surface of the SiC particulate. SiO_2, can be reduced by Mg during heating. With the increase in volume of SiC particulates, more brittle MgO layers are formed leading to a decrease in tensile strength.

In addition, Mg also reacts with SiC particulates to form an interfacial reaction compound of Mg_2Si at the interface between the Mg matrix and SiC. The presence of Mg_2Si layer could also weaken the interfacial bonding and cause early debonding of the particulates upon loading.

The increase in Young's modulus is not surprised. It can be explained by the Tsai-Halpin model [21] which takes the geometry of the reinforcement into account:

$$E_C = \frac{E_M(1 + 2SqV_P)}{1 - qV_P} \tag{3}$$

$$q = \frac{(E_P/E_M) - 1}{(E_P/E_M) + 2S} \tag{4}$$

where E_C, E_M, and E_P are respectively the Young's moduli of the composite, matrix and particles, V_P, volume fraction of particles, and S, particle aspect ratio.

It can be seen that basically the modulus of the MMC is a function of the Young's modulus of Mg matrix, SiC as well as volume percentage of SiC. Increase either in E_p or V_p will lead to an increase in Young's modulus of the MMC.

Ductility of the MAed specimens was significantly reduced with the increase in the amount of SiC (Fig. 14). This reduction in ductility could be explained by the initiation of debonding between the matrix and the SiC reinforcement by producing voids and microcracks and by weakening the bonding. The latter could be caused by the reaction compounds or poor interfacing due to low extrusion ratio. The other explanation could be that the SiC particulates are being incorporated into the MMC along the grain boundary of the Mg matrix during the ball milling process and these acted as obstacles to the diffusion across the grain boundary and restricted the movement of dislocations. Hence, as SiC content increased, the hindrance effect of SiC correspondingly increased, resulting in the subsequent reduction in the ductility of the MMC.

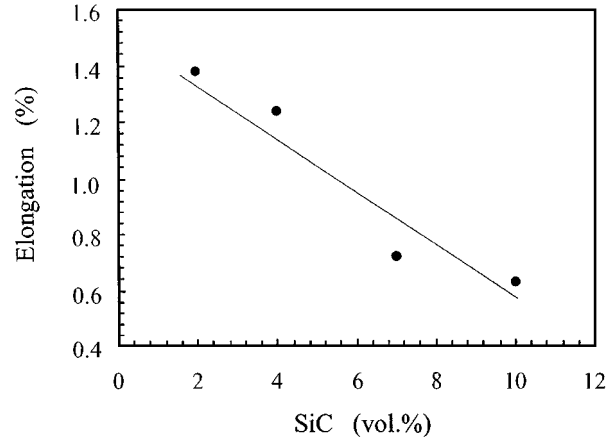

Figure 14 Elongation as a function of volume percentage of SiC.

3.4. Fractography

Fractography of the non-MAed MMC is given in Fig. 15. It can be seen that fracture occurred due mainly to debonding at the matrix and SiC particulate interface. The presence of segregation of SiC particulates in the Mg matrix leads to separation of the particulates since

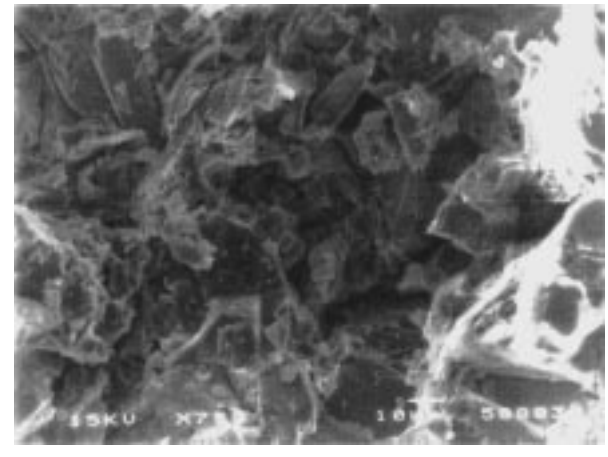

(a)

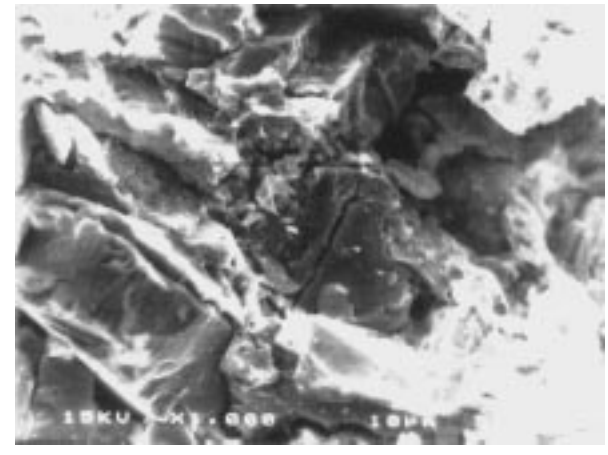

(b)

Figure 15 Fractograph of AZ91 MMCs reinforced with different size of SiC: (a) 15 μm and (b) 50 μm.

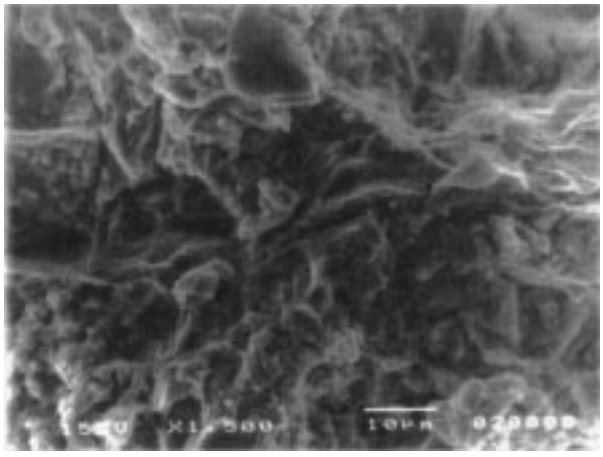

(a)

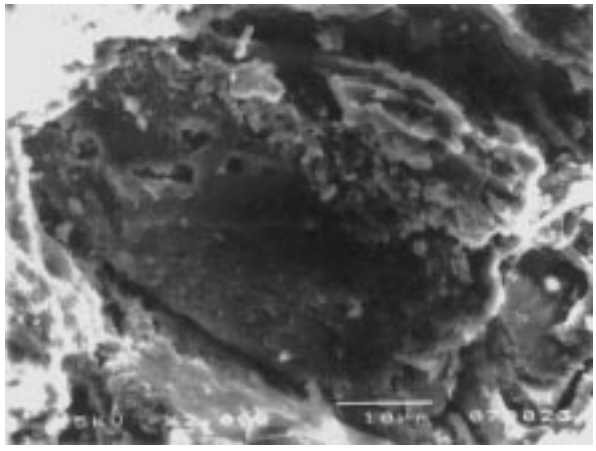

(b)

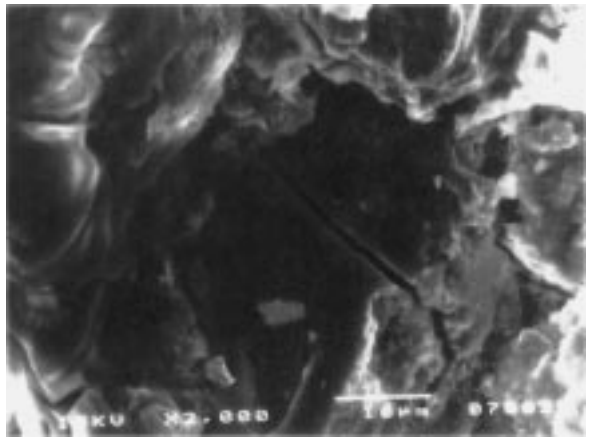

(c)

Figure 16 Fractograph of AZ91 MMCs reinfiorced with different amount of SiC: (a) 2 vol.%SiC, (b) 7 vol.%SiC and (c) 10 vol.%SiC.

there is little bonding between them. Fracture mode changed from initial debonding to inter-particulate fracture. Intergranular fractures along the grain boundaries can also be observed. This is closely related to the $Mg_{17}Al_{12}$ precipitates located along the grain boundaries. The presence of the precipitates weakens the grain boundaries.

For the smaller size particulates, e.g. 15 to 25 μm, there is very little particle cracking; the failure mechanism appeared to be particle-matrix interface decohesion (Fig. 15a). As discussed earlier, at least two reactant layers at the interface between Mg matrix and SiC have been reported, namely, MgO and Mg_2Si. Since both of these are brittle, it is not surprising that interfacial decohesion takes place before particle cracking.

For larger particles size in the range of 38 μm and 50 μ, damage was confined mainly in particle clusters (Fig. 15b). High tensile stresses in the particle clusters resulting from constrained plastic flow and triaxial stress intensification led to damage by particle cracking as well as interface decohesion.

Fig. 16 shows the fracture morphologies of MAed MMCs. For the MMCs reinforced with 2 and 4% SiC, crack propagation took place by the micro-void coalescence of the interconnecting matrix at interface (Fig. 16a). For the 7% (Fig. 16b) and 10% (Fig. 16c) SiC reinforced material, particle-matrix debonding and particle cracking can clearly be seen from the fractographs. These failure modes are the results of localized stress concentration developed at the interface. As SiC content increases it appears that defects like reaction compound Mg_2Si and brittle intermetallic compound $Al_{12}Mg_{17}$ at the interface between the matrix and the particles and at the grain boundaries respectively begin to play a dominant role not only on the fracture morphologies but also the mechanical properties of the composites

4. Conclusions

AZ91/SiC composite materials have been fabricated via powder metallurgy and mechanical alloying techniques. The composites showed a slight decrease in yield and tensile strengths when the size of SiC particulate was increased. An improvement in yield and tensile strengths was however observed after mechanical alloying.

The increase in mechanical properties of the mechanically alloyed composite could be attributed to grain refinement, homogeneous distribution of SiC particlates and small intermetallic precipitates.

The present results showed that the increase in amount of SiC in the composite led to a decrease in yield and tensile strengths. This observation was associated to interface reaction between the reinforcement and the Mg matrix. The interfacial reaction between Mg, SiC and SiO_2 during sintering and extrusion resulted in a brittle interface, which finally led to early debonding between the reinforcement and the matrix.

Acknowledgement

The present project is financially supported by The National University of Singapore under research grants, RP970654 and RP 981633.

References

1. R. OAKLEY, R. F. COCHRANE and R. STEVENS, *Key Eng. Mater*. **104**–**107** (1995) 387.
2. K. U. KAINER, in "Magnesium Alloys and Their Applications," edited by B. L. Mordike and F. Hehmann (DGM Informationsgesellschaft, Oberursel, 1992) p. 415.
3. U. ROOS, K. U. KAINER and B. L. MORDIKE, in Proc. of the Powder Metallurgy World Congress PM'94 (Société Française de Métallurgie et de Matériaux, Paris, France, 1994) Vol. 3, p. 2249.
4. K. U. KAINER and E. BÖHM, in Proc. of 29th Int. Symp. on Automotive Technology and Automation, edited by D. Roller (Automotive Automation Ltd., Croydon, GB, 1996) p. 653.

5. J. S. H. LO and G. J. C. CARPENTER, in Proc. ICCM11, Gold Coast, Australia, 14–17 July 1997, edited by M. L. Scotte (Publ. Australian Composite Structures Sciety, 1997) p. 688.
6. D. J. LLOYD, *Inter. Mater. Rev.* **39**(1) (1994) 1.
7. R. MOLINS, J. D. BATOUT and Y. BIENVENU, *Mater. Sci. Eng.* **A135** (1991) 111.
8. G . POLLARD, *Mater. Sci.* **28** (1993) 4427.
9. J. SCHRODER, K. U. KAINER and B. L. MORDIKE, in Proc. 2nd Inter. Confer. on Adv. Mater. and Processes, EURO MAT91, Vol. 2, Adv. Structural Mater., edited by T. W. Clyue and P. J. Withers (Publ. The Inst. of Mater., 1991) Vol. 2, p. 81.
10. J. S. BENJAMIN, Metall. Trans., Vol. 1 (1970) 2943.
11. R. F. SINGER, W. C. OLIVER and W. D. NIX, *Metall. Trans.* **11A** (1980) 1895.
12. G. JANGG, M. SLESAR, M. BESTERCI, J. DURISIN and K. SCHRODER, *Powder Metall. Inter*. **21** (1989) 25.
13. C. C. KOCH, O. B. GAVIN, C. G. MCKAMEY and J. O. SCARBOROUGH, *Appl.Phys. Lett.* **43** (1983) 1017.
14. C. C. KOCH, *Nanostructured Mater*. **2** (1993) 109.
15. X. P. NIU and LI LU, *Adv. Performance Mater.* **3** (1997) 275.
16. G. J. SHEN, Y. CAI and J. Z. SONG, *J. Mater. Sci. Lett.* **15** (1996) 2058.
17. LI YICHUN and AN XIYONG, *Rare Metal* **13**(2) (1994) 108.
18. J. K. KEK, L. LU and M. O. LAI, in ICCM 11, Gold Coast, Australia, 14–17 July 1997, edited by M. L. Scotte (Publ. Australian Composite Structures Sciety, 1997) p. 250.
19. M. MABUCHI, T. ASAHINA, K. KUBOTA and K. HIGASHI, in Proc. of the 3rd Inter. Mg Confer., 10–12 April 1996, Manchester, UK, edited by G. W. Lorimer, p. 439.
20. R. ARMSTRONG, I. CODD, R. M. DOUTHWAITE and N. J. PETCH, *Philos. Mag.* **7** (1962) 45.
21. J. C. HALPIN, in "Primer on Composite Materials: Analysis" (Technomic Pub., rev. edn., 1984, Lancaster, PA, U.S.A.) p. 130.

Received 12 November 1999
and accepted 30 March 2000